3D and 2D Finite Element Analysis in Soft Tissue Cutting for Haptic Display*

Teeranoot Chanthasopeephan, Jaydev P. Desai†, and Alan C. W. Lau
Program for Robotics, Intelligent Sensing, and Mechatronics (PRISM) Laboratory
Drexel University
Philadelphia, PA 19104
Email: {teeranoo, desai, alau}@coe.drexel.edu

Abstract - *Real-time medical simulation for robotic surgery planning and surgery training requires realistic yet computationally fast models of the mechanical behavior of soft tissue. This paper presents a study to develop such a model to enable fast haptics display in simulation of soft-tissue cutting. An apparatus was developed and experiments were conducted to generate force-displacement data for cutting of soft tissue such as pig liver. The force-displacement curve of cutting pig liver revealed a characteristic pattern: the overall curve is formed by repeating units consisting of a local deformation segment followed by a local crack-growth segment. The modeling effort reported here focused on characterizing the tissue in the local deformation segment in a way suitable for fast haptic display. The deformation resistance of the tissue was quantified in terms of the local effective modulus (LEM) consistent with experimental force-displacement data. An algorithm was developed to determine LEM by solving an inverse problem with iterative finite element models. To enable faster simulation of cutting of a three-dimensional (3D) liver specimen of naturally varying thickness, three levels of model order reduction were studied. Firstly, a 3D quadratic-element model reduced to uniform thickness but otherwise haptics-equivalent (have identical force-displacement feedback) to a 3D model with varying thickness matching that of the liver was used. Next, haptics-equivalent 2D quadratic-element models were used. Finally, haptics-equivalent 2D linear-element models were used. These three models had a model reduction in the ratio of 1.0:0.3:0.04 but all preserved the same input-output (displacement, force) behavior measured in the experiments. The values of the LEM determined using the three levels of model reduction are close to one another. Additionally, the variation of the LEM with cutting speed was determined. The values of LEM decreased as the cutting speed increased.*

Index Terms—Haptic display, Soft tissue cutting, Local effective modulus.

*This work was supported in part by National Science Foundation grants EIA-0312709, and CAREER award IIS 0133471.
†Corresponding author.

I. INTRODUCTION

Modeling deformable soft tissue is essential for accurate surgical simulation. A realistic model of soft tissue can provide accurate force feedback to the user through a haptic interface device. The mechanical characteristics of living tissue such as liver are highly nonlinear and complicated. In real-time simulation requiring fast and accurate force feedback, the calculation time plays an equally important role as the realism of the model. Our objective here is to study haptically realistic yet computationally fast models suitable for r*eal-time medical simulation for robotic surgery planning and surgery training.*

Various approaches were used to study the properties and behavior of soft tissue. Fung [1] described soft tissue as nonlinear, inhomogeneous and viscoelastic. Kerdok and Howe et al [2] used a truth cube observe soft tissue deformation and compared it to results from finite element model. Hu and Desai studied the large-deformation tissue behavior in compression test [3]. Finite element method (FEM) [4] had been used as a tool to determine the physical behavior in soft tissue simulation under mechanical constraints. Bro-Nilsen and Cotin et al [5, 6] used 3D volumetric finite element model for surgery simulation. To render the 3D continuum FE model of tetrahedral elements capable for real time simulation, they reduced the order of the model by statically condensing out the internal degree of freedom (dof) while keeping only the dof associated with surface nodes. James and Pai [7] used boundary integral formulation and discretized the geometry with boundary element method (BEM) in real-time simulation of the deformation of linear elastic objects. For linear elastic deformation, the solution can be attained by the superposition of pre-determined response of unit loading (influence functions or Green's functions) and James and Pai implemented this feature with a low order updating algorithm. Zhuang and Canny [8] proposed finite element models to speed up the simulation of the large deformation of 3D objects subject to dynamics and static loads. For statics analysis, their model achieved model reduction primarily with the use of a graded mesh consisting of small elements at the exterior but large element in the interior. De and co-workers [9] proposed to use finite spheres method (FSM) as a meshless scheme for real-time medical simulation. The governing equations of elasticity were numerically solved by the method of collocation at the nodal points, which were placed near the surgical tool tip [10].

In our study, we proposed to achieve reality-based simulation by using material properties consistent with experimentally measured force-displacement data. To attain fast but realistic force feedback in real-time simulation, we used coarse-mesh finite element model while retaining the realistic overall force-displacement behavior by using local effective modulus (LEM), which are consistent with experimental results. To foster reduction of the computation effect and faster simulation, we studied three levels of 3D/2D model order reduction. The goal in model order reduction is to preserve the overall input-output (overall displacement, force) behavior while eliminating the internal complexity of the model.

In this paper, Section II describes the experimental equipment and procedure. Section III presents the algorithm to determine LEM by solving an inverse problem with iterative finite element method. Section IV presents the three levels of 3D and 2D model order reduction studied. Section V shows the results and Sections VI presents the conclusions and remarks.

II. Soft Tissue Cutting Experiments

2.1 The soft tissue cutting apparatus

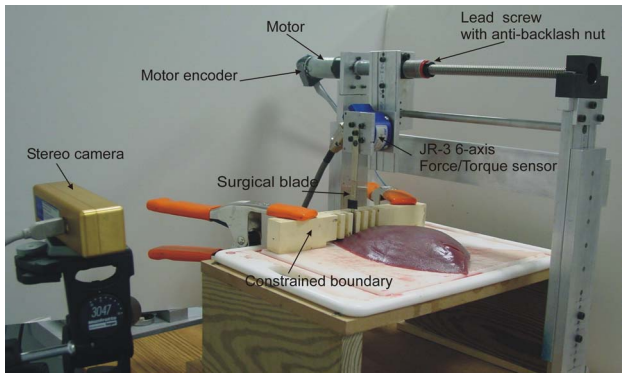

Figure 1. Experimental setup for measuring the cutting forces and grabbing images during liver cutting.

The soft-tissue cutting apparatus consists of a scalpel-blade cutting subsystem, a computer control subsystem, a digital data-acquisition subsystem, and a data post-processing subsystem (see figure 1) [11]. The test equipment to measure the liver cutting forces was designed to have a variable cutting speed to measure the effect of cutting speed on cutting forces within the specimen (speeds can be varied from 0 to 3.81cm/second). The constrained boundary shown in the figure was designed to simulate the attachment of the liver on one end as in a human body (such as the attachment to the diaphragm). The cutting mechanism consists of two vertical supports, a lead screw assembly with a geared DC motor and an incremental encoder (manufactured by Maxon Motors, model A-max32 with planetary gearhead GP 32C and digital encoder HEDL 55 with line driver RS 422), and a JR3 precision 6-axis force/torque sensor (model 85M35A-I40, with worst case resolution of 0.05 N in Fx and Fy, 0.1 N in Fz and 0.00315 Nm in Tx, Ty and Tz) to which a surgeon's scalpel is attached.

We used #10 Bard-Parker stainless steel surgical blade in our experimental studies, consistent with what is used by surgeons. The cutting blade traverses linearly based on the rotary motion of the DC motor. An anti-backlash nut connects the lead screw to the force sensor. The scalpel was screwed to the force sensor and the force sensor was mounted on an aluminum plate with one end attached to the anti-backlash nut traveling along the lead screw and the other end on a lower guiding shaft (parallel to the lead screw) with a linear bearing to provide low friction linear travel. The design and construction of the cutting assembly ensured that the system was sufficiently rigid with no backlash so that the forces recorded by the force sensor are those obtained by cutting the tissue alone. A Bumblebee stereo camera system is arranged at 30cm in front of the experimental setup. The dSPACE DS1103 controller board (manufactured by dSPACE, Inc.) recorded the position and force data from the motor's encoder and force sensor in real-time along with grabbing images at the rate of 13 frames/second. We have implemented a proportional + derivative (PD) controller to enable precise movement of the motor (and hence the cutting blade during cutting tasks).

2.2 Experimental procedure for measuring liver cutting forces

Since the experiments were performed on ex-vivo liver tissue, the preparation of the tissue before the experiment helped maintain the properties of the tissue as close as possible to the in-vivo properties. We transported the liver from freshly slaughtered pigs to our laboratory within 2 hours post mortem. The liver tissue sample was not preconditioned because in surgery, the cutting forces experienced by the surgeon are on non-preconditioned tissues. Before starting the experiment, we cut the pig's liver into specimens of size 8x15x2.5cm. The outer encapsulated surface was not cut since we were interested in measuring the cutting forces on the liver. A bar of rectangular shape made of machineable plastic with an array of small nails clamped at the bottom end penetrated through one edge of the liver specimen to simulate a single constrained boundary surface. While this is not an exact replication of the boundary conditions for a human liver (which is partially attached on one end to the diaphragm) this is none-the-less a valid simplification for our initial tests and model (based on our discussions with surgeon collaborators).

2.3 Characteristics of the cutting force-displacement curve

The experimentally measured force-displacement curve of pig-liver cutting showed a characteristic pattern. The overall force-displacement curve is formed by repeating units each consisting of a local deformation segment followed by a local crack-growth segment (Figure 2). In the each deformation segment the force increment increases linearly with the displacement increment (see insert of Figure 2). The crack-growth segment shows an instantaneous unloading (load drop). Each visually observed localized blade cut on the tissue clearly corresponded to a sudden drop of the force measured by the force sensor. A filtering procedure has been developed to post-process the data to produce a force versus cut-length curve clearly illustrating the "hilltops" and "valleys" of the sequence of localized loading and unloading in the tissue specimen during cutting.

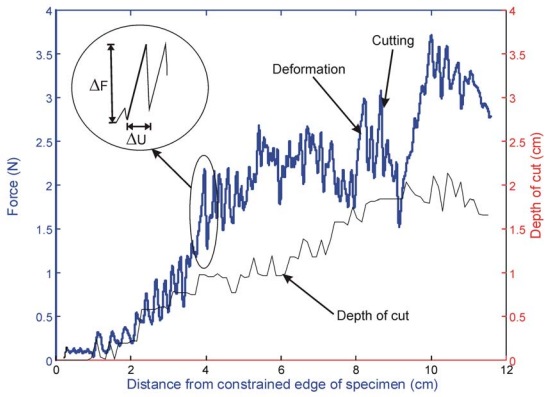

Figure 2. Raw experimental data from liver cutting. Typical repeating units of linear loading segment followed by sudden unloading segment are shown.

2.4 Stereo-image determination of depth-of- cut

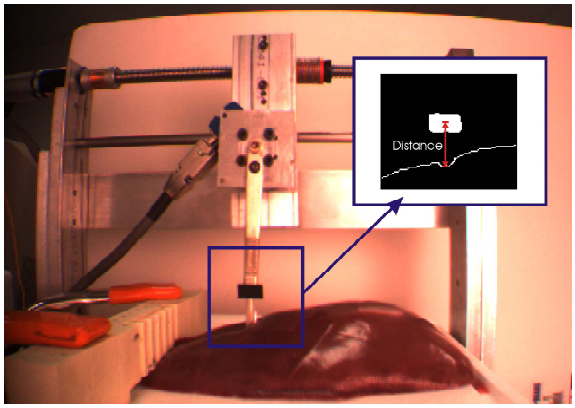

Figure 3. Snap shot from the stereo camera.

As is expected, during the cutting process the depth of the blade embedded in the tissue affects the magnitude of the cutting force encountered by the blade (see Figures 3 insert). The depth of cut was measured using optical stero imaging, and was used to obtain the normalized cutting force (per unit depth of cut). We used stero images to analyze how deep the blade was inside the liver specimen during cutting. A Bumblebee two-lens stereovision camera system grabbed snap shots of cutting (Figure 3) at 13 frames/second. The images were analyzed offline using Matlab6.5 with image processing toolbox.

After obtaining snap shots, we performed post processing by tracking the center of the black rectangular box (Figure 3), which was on the top of the cutting blade. Then using edge detection, we were able to detect the liver surface as shown in Figure 3 insert. The distance from the center of the rectangular box and the surface of the liver is measured in term of pixel. Since the position of the center of the box to the end of the blade is 4 cm, we determine the depth of cut through conversion from pixel to distance in centimeter.

III. DETERMINATION OF LOCAL EFFECTIVE MODULUS

3.1 Finite element model for computing the local effective modulus (LEM)

It is desirable to construct a predictive computational model that can simulate the cutting process and predict the mechanical response (cutting force versus cutting-blade displacement characteristics) of liver cutting. To be of real-time application, this simulation model should not be computationally intensive yet still capture the real force-displacement behavior. We propose to use coarse-mesh finite element (FE) models and effective material properties consistent with experimentally measured force-displacement curve.

Five 3D and 2D coarse-mesh finite element models with three different levels of model simplification were used in this study. The following three levels of model reduction are constructed to simplify the model but retain the overall force-displacement response behavior: a) a thickness-normalized 3D model with 480 quadratic elements, b) 2D models with 120-element quadratic elements, and c) 2D models with 120 linear elements. Additionally, in each of the 2D models two sub-model varieties were used: plane-stress elements and plane-strain elements. While using this coarse-mesh FE model for simulation via haptic feedback device, the contact force feedback felt by the surgeon must be accurate. To ensure that these coarse-mesh FE models can preserve the experimentally measured force-displacement characteristics, we need to use an effective modulus that is consistent with the experimental data. We describe below the procedure to determine this local

effective modulus (LEM). The finite element analysis was conducted with the ABAQUS 6.3 software [12].

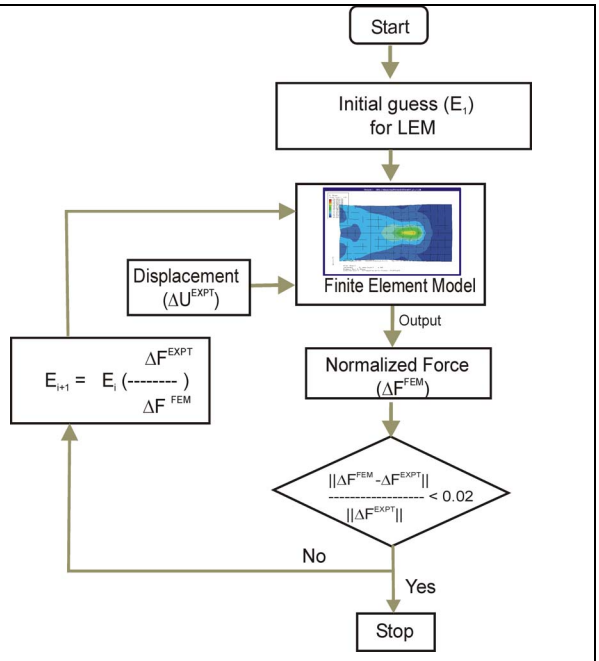

Figure 4. Flow chart for determination of self consistent effective modulus.

The LEM consistent with experimental data can be determined by solving an inverse problem formulated with the data from the linear loading segments (Figure 2 insert) and a coarse-mesh FE model. After obtaining the force-displacement curve from the experiment, we filtered the data followed by identifying each linear deformation segment shown in Figure 2 insert. To simulate each of the linear deformation segments with local displacement increment ΔU and force increment ΔF, we used either a 3D finite element model with unit thickness or a 2D finite element model. As looked at from above, the FE mesh we used consisted of a left half and a right half of identical elements and joined at the adjoining center line. At the centerline, the contacting nodes from the left half and right half were "tied" with multi-point constraint (MPC) equations. Hence, the two halves formed a continuous solid. During the analysis, as we simulated the scalpel cut along the centerline of the specimen step by step, we would "untie" the adjoining nodes element by element. Hence the cut or crack grew step by step during the process of FE analysis.

Since our FE model is of unit thickness, we first divided the experimentally measured force increment ΔF by the depth of the blade embedded in the tissue at that instant of cutting (see section 2.4 above.) The result is a ΔF per unit length of the blade cutting the tissue. We denote this depth-normalized or thickness-normalized force increment as ΔF^{exp}.

Figure 4 shows the flowchart of our determination of the LEM for each deformation segment of the force-displacement curve (Figure 2). For each deformation segment, we conducted a linear elastic FEM analysis with Poisson's ratio 0.3 and an initial modulus of arbitrary magnitude E_1. We applied the experimental measured displacement increment ΔU^{exp} of the deformation segment to the FEM node that was in contact with the cutting blade. We performed the FEM analysis and compared the FEM computed force increment ΔF^{FEM} of that node to the experimentally measured ΔF^{exp}.

In the first iteration, ΔF^{FEM} will not be equal to ΔF^{exp}. To start the next iteration, we updated the new value of the effective modulus to E_2 with equation (1) and repeated the iteration process.

$$E_{i+1} = E_i \left(\frac{\Delta F^{EXPT}}{\Delta F^{FEM}}\right) \qquad for \quad i = 1,2,..... \tag{1}$$

This process continued until ΔF^{FEM} of a new iteration was "equal to" the normalized force increment ΔF^{exp} as determined by the convergence criterion of equation (2).

$$\frac{\left\| \Delta F^{FEM} - \Delta F^{EXPT} \right\|}{\Delta F^{EXPT}} \leq 0.02 \tag{2}$$

The final E value so determined is the effective modulus at the location in the tissue where the cutting blade was in contact with the tissue, $E^{effective}$. We denoted this quantity as the local effective modulus (LEM).

The data of the experimentally measured force increment ΔF has incorporated into it the varying depth of cut, which depends on the instantaneous location of the scalpel and the natural bulge of the liver specimen. Consequently, the local effective modulus LEM has incorporated with it the influence of the natural bulge in thickness of the liver because it is derived from the actual force increment ΔF sensed by the scalpel as it traversed liver portions of varying thickness.

With LEM determined via inverse analyses from experimental data, we can conduct surgery simulation by forming a coarse-mesh FEM model of the liver, assign the elements in the FEM model with their respective $E^{effective}$ and use that FEM model to virtually simulate various patterns of liver cutting and can vary the cutting parameters such as cutting speed and cutting angle. Such an FEM model embedded with self-consistent local effective modulus would be able to predict a cutting-force versus displacement characteristics in each of the monotonic loading segments consistent with experimentally-measured values, should actual experiment of that particular cutting pattern be performed. In this way, a surgeon trainee using a surgery-training simulator will see the length of the cut grow and feel the cutting forces via a haptic feedback device.

IV. THREE LEVELS OF MODEL ORDER REDUCTION

To have faster simulation yet have realistic force feedback, our goal is to use model order reduction to simplify the internal complexity of the model and simultaneously preserve the overall input-output (displacement-force) behavior. The realistic force feedback part is attained via using LEM. The speed of the simulation depends on how much order reduction the model can attain. We studied three levels of model order reduction.

4.1 3D quadratic-element model with unit thickness

The common way to construct a 3D model of the liver is to generate a 3D continuum shape reflecting the actual shape of the liver and discretize the geometry into continuum elements. To provide haptic feedback in surgery simulation, it is most important that the surgeon trainee receive accurate force feedback and also sees the instantaneous length of the cut. It is less important to see the actual thickness of the liver. We can thus simplify the general 3D model into a 3D model with unit thickness, and use LEM derived from thickness-normalized ΔF^{exp}. Figure 5a shows such a model. The size of the specimen was 8 cm x 15cm while the element size was 1 cm x 1cm x 0.25cm. The model consists of 8 elements in the width dimension, 15 elements in the length dimension, and 4 elements in the thickness dimension. These 480-element model are constructed with quadratic continuum elements (20-node brick elements of the Serendipity family of isoperimetric elements). The displacements can vary quadratically, and strain and stress can vary linearly, in each element. The cutting path with the "tied" double nodes (section 3) along the cut plane (the plane along which the scalpel with travel in the liver) is along the center line. There are four columns of elements to its left of the cutting path and four columns of elements to its right This mesh has 2830 nodes and 8490 degrees of freedom (8490 equations).

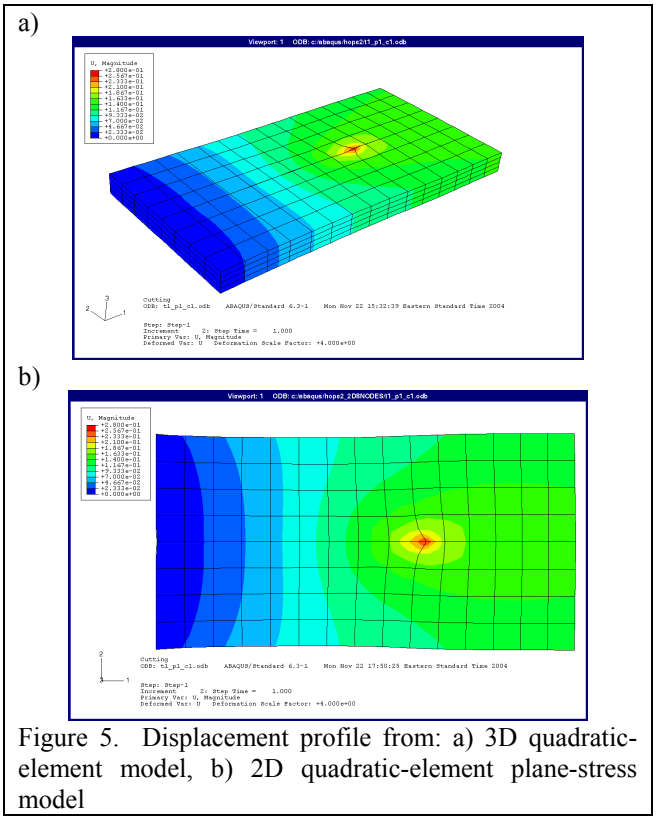

Figure 5. Displacement profile from: a) 3D quadratic-element model, b) 2D quadratic-element plane-stress model

During the simulation of the cutting process, the tied nodes on the cutting path were untied once the cut already occurred. Since the model should replicate the behavior of the liver during cutting as much as possible, the un-tied nodes were constrained to move along the axis so that the two cut parts would not overlap. At the leading edge, the model was constrained by fixed nodes along the edge. The constraints were intended to replicate how we constrained the liver specimen during cutting experiment through the nails array clamped at the leading edge.

4.2 2D quadratic-element models

To reduce the model order further, we reduced the 3D quadratic model of section 5.1 to a 2D model with quadratic elements. These are 8-node quadrilateral elements of the Serendipity isoparametric element family. The inplane displacement can vary quadratically, and the inplane strains can vary linearly, in the element. We conducted analysis both with a plane-stress elements and plane strain elements. The 2D mesh (Figure 5b) consists of 120 elements of 1cm x 1cm size filling the 8cm x15cm x 1cm specimen. The mesh has 8 elements in the width dimension, and 15 elements in the length dimension. There are 438 nodes and 876 degrees of freedom (876 equations).

4.3 2D linear-element models

To further reduce the 2D models above, we conducted plane-stress analysis and plane-strain analysis with 2D linear elements. The mesh looks identical to that in Figure 5b. The difference with section 5.2 is the elements do not have mid-side node. Four-node quadrilateral elements of the Serendipity element family are used. The displacements can vary linearly, and the strains and stress are constant, in each element. The model has 120 elements, 160 nodes and 320 degrees of freedom (320 equations).

V. RESULTS

We performed a quasi-static analysis using ABAQUS finite element software version 6.3-1. Since the deformation during deformation segment appeared to be linear (Figure 2 insert), we conducted isotropic linear elastic analysis. The poison ratio was assumed to be 0.3.

With experimental force-displacement data from 0.15 inch/sec cutting speed, we performed analysis to determine LEM using the 3D-quadrati-element model (20-nodes element) and 2D-quadrtic-element model (8-node elements). Along a cutting path, we determined the LEM corresponded to each deformation segment. The values of the LEM so determined are shown in Figures 6, 7 and Table 1.

Distance from constrained edge (cm)	LEM from 3D quadratic FE model (N/m^2)	LEM from 2D quadratic FE models		Ratio of LEM from 2D to that from 3D model	
		Plane-stress (N/m^2)	Plane - strain (N/m^2)	Plane-stress / 3D model	Plane-strain / 3D model
2.15	3200	3400	3100	0.97	1.1
2.90	7300	7900	7300	1.0	1.09
4.08	9700	10100	9200	0.96	1.04
4.75	36900	37800	35000	0.94	1.02
5.14	29700	30500	28100	0.94	1.02
5.64	37400	38900	35700	0.95	1.04
6.09	18200	18600	17200	0.94	1.0
6.61	60400	61500	56700	0.94	1.02
6.90	50000	50800	46900	0.94	1.02

Table 1. Comparison of LEM determined from 3D quadratic-element model and 2D-quadratic-element plane-stress model and plane-strain model.

With the same force-displacement during the deformation, we performed similar analysis using 2D-linear-element (4-node elements) in plane-stress model and plane-strain model. Results are shown in Figures 6, 7 and Table 2. Results from Figures 6, 7, Tables 1 and 2 show that the LEM based on 3D model falls in the bracket between the LEM from 2D plane-stress and plane-strain models. The results help verify that the 2D plane-stress and plane-strain model can produce equally good results for LEM as the 3D model.

Distance from constrained edge (cm)	LEM from 3D quadratic FE model (N/m^2)	LEM from 2D linear FE models		Ratio of LEM from 2D to that from 3D model	
		Plane-stress (N/m^2)	Plane - strain (N/m^2)	Plane-stress/ 3D	Plane-strain/ 3D
2.15	3200	5000	4700	1.57	1.47
2.90	7300	8800	8100	1.21	1.12
4.08	9700	10500	9700	1.09	1.00
4.75	36900	39000	36100	1.06	0.98
5.14	29700	31300	28800	1.05	0.97
5.64	37400	39100	36000	1.04	0.96
6.09	18200	18900	17500	1.04	0.96
6.61	60400	62500	57600	1.04	0.95
6.90	50000	51600	47600	1.03	0.95

Table 2. Comparison of LEM determined from 3D quadratic-element model and 2D linear-element plane-stress model and plane-strain model.

From the perspective of computational effort, there is a significant difference among these models – the size (or order) of the model and the computational efforts needed to solve them. Table 3 shows a comparison among these models in terms of the total number of elements, total number of nodes and total number of equations. Using the number of equations as a measure of the size (or order) of the model, the relative size of the 3D-quadratic-element model to 2D-quadratic-element model to 2D-linear-element model is 1.0:0.3:0.04. It is expected that compared with the 3D-quadratic-element model, the 2D-quadratic-model will be one order of magnitude less computational-intensive. Further, the 2D-linear-element model is only about 4% as computational intensive as the 3D-quadratic model. Indeed, our computation time for the 2D-linear-model is about 4% of that of the 3D-quadratic-element model.

FE Model	3D quadratic elements	2D quadratic elements	2D linear elements
Number of elements	480	120	120
Number of nodes	2830	438	160
Number of equations	8490	876	320
Relative model size	1.0	0.1	0.04

Table 3. Comparison among the 3D and 2D models.

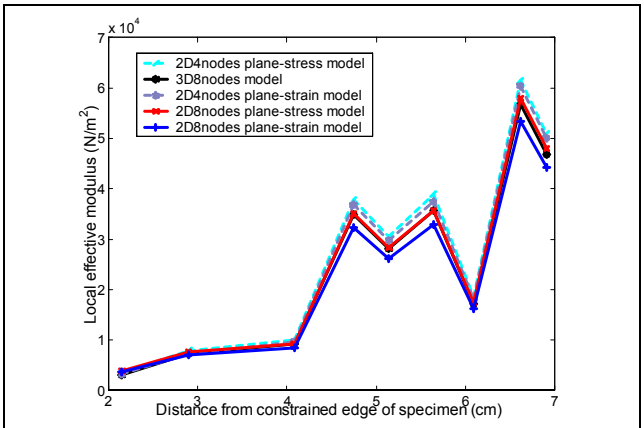

Figure 6. Comparison between the values of LEM from 3D-quadratic element model, 2D-quadratic-element models and the 2D-linear-element models

Additionally, we used the 3D-quadratic-element model to conduct a parametric study for the effect of cutting speed on the deformation resistance (the LEM) of the liver tissue. Experimental force-displacement data were collected for seven cutting speeds (0.10cm/sec, 0.38cm/sec, 0.89cm/sec, 1.27cm/sec, 1.65cm/sec, 2.16cm/sec, and 2.54 cm/sec). LEM were determined for each of these cutting speeds. The average value of the LEM for each cutting speed was calculated. Figure 8 shows the average of the LEM for each of the cutting speeds. It is apparent that the deformation resistant as measured by LEM decreases as the cutting speed increases.

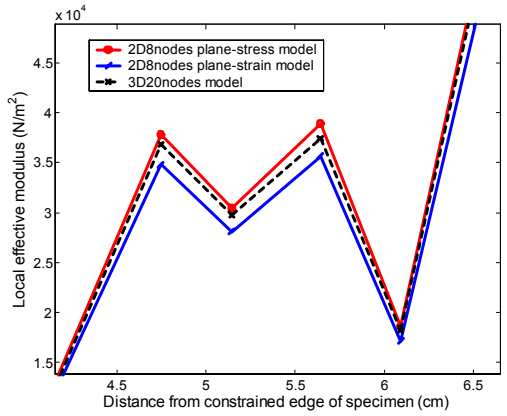

Figure 7. Magnified view of a portion of Figure 6a showing the LEM from quadratic-element model of 3D analysis is bracketed between LEM determined from 2D plane-stress analysis and plane-strain analysis.

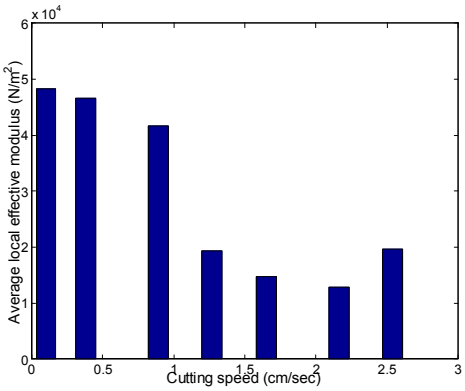

Figure 8. Average LEM based on 3D model at various cutting speeds.

VI. Conclusions and Remarks

In this paper, we presented the experiments to generate the force-displacement characteristic during the cutting of soft tissue. The force-displacement curve consists of two repeating basic building blocks: a local deformation segment followed by a local crack growth segment. A procedure was developed to determine the local effective modulus during the local deformation segment of the force-displacement curve.

For real-time medical simulation requiring accurate haptic feedback, it is important to have reality-based models that are fast (computationally non-intensive) but still preserve the actual overall force-displacement behavior. Several 3D and 2D finite element models with three levels of model order reduction were studied. These model order reductions simplify the internal complexities of the model while preserving the overall input-output (displacement-force) behavior. All these models can determine the local effective modulus equally well, and the results of the 3D model are bracketed by results from the 2D plane-stress model and 2D plane-strain model. .

A plane-stress FE model is most appropriate for simulating the cutting of very thin liver specimens in which the through-thickness stress is negligible (i.e. completely unconstrained in the thickness dimension and allows free through-thickness deformation). A plane-strain FE model is most appropriate for very thick liver specimens in which the through-thickness strain is negligible (i.e. fully constrained in the thickness dimension and does not allowed to through-thickness deformation). It is reasonable that the results of the 3D model falls in-between the results from the two limiting case of plane-stress and plane-strain models

With regard to computation effort required, there is a significant difference among these models. The computation effort required for the 2D-quadratic-element model is one order of magnitude less that required for the 3D-quadratic-element model. The computation effort for the 2D-linear-element model is two orders of magnitude smaller that that of the 3D-quadratic-element model.

A parametric study for the effect of cutting speed on the local effective modulus of pig-liver cutting revealed that the apparent deformation resistance of the pig-liver tends to decrease as the cutting speed increases.

VII. References

1. Fung, Y.C., *Biomechanics: Mechanical properties of living tissues*. Second edition ed. 1993, New York: Springer-Verlag.
2. Kerdok, A.E., et al., *Truth cube: Establishing physical standards for real time soft tissue simulation.* Medical Image Analysis, 2003. **7**: p. 283-291.
3. Hu, T. and J.P. Desai. *Characterization of soft-tissue material properties: Large deformation analysis*. in *Second International Symposium on Medical Simulation - Emerging Science|Enabling Technologies*. 2004. Boston, MA.
4. Bathe, K., *Finite Element Procedures*. 1996, Englewood Cliffs: Prentice Hall.
5. Cotin, S., H. Delingette, and N. Ayache, *Real-Time elastic deformations of soft tissue for surgery simulation.* IEEE Transactions On Visualization and Computer Graphics, 1999. **5**(1): p. 62-73.
6. Bro-Nilsen, M. and S. Cotin, *Real time volumetric deformable models for surgery simulation using finite elements and condensation.* Computer Graphics Forum, 1996. **15**(3): p. 57-66.

7. James, D. and D. Pai. *ARTDEFO: Accurate real time deformable objects*. in *Computer Graphics (SIGGRAPH)*. 1999.
8. Zhuang, Y. and J. Canny. *Real-time simulation of physically realistic global deformation*. in *SIGGRAPH99 Sketches and Applications*. 1999. Los Angeles, CA.
9. De, S., J. Kim, and M.A. Srinivasan. *A meshless numerical technique for physically based real-time medical simulations*. in *Medicine meets virtual reality*. 2001.
10. De, S., J.W. Hong, and K.J. Bathe, *On the method of finite spheres in applications: towards the use with ADINA and a surgical simulator.* Computational Mechanics, 2003. **31**: p. 27-37.
11. Chanthasopeephan, T., J.P. Desai, and A.C.W. Lau, *Measuring Forces in Liver Cutting: New Equipment and Experimental Results.* Annals of Biomedical Engineering, 2003. **31**(11): p. In Press.
12. ABAQUS, *ABAQUS version 6.3*. 2003, ABAQUS Inc, Pawtucket, Rhode Island, 2004.